ACS OMEGA

http://pubs.acs.org/journal/acsodf

Article

# Binary System of Polyethylene Glycol 200 (1) + 3-Dimethylamino-1-propylamine (2) for $CO_2$ Absorption: Thermophysical Properties and Spectroscopic Study

Xiaoqing Yang,[†] Zimin Liu,[†] Tianxiang Zhao,* Jiarui Gu, Fei Liu,* and Jianxin Cao

Cite This: *ACS Omega* 2021, 6, 9898−9909

Read Online

ACCESS | Metrics & More | Article Recommendations | Supporting Information

**ABSTRACT:** As the concentration of $CO_2$ in the atmosphere keeps increasing, the development of a highly efficient $CO_2$ absorbent is highly desired. In this work, a binary mixture system of polyethylene glycol 200 (PEG 200) (**1**) + 3-dimethylamino-propylamine (DMAPA) (**2**) was used for $CO_2$ absorption. Considering the importance of thermophysical properties to binary solutions, the densities and viscosities of the PEG 200 (**1**) + DMAPA (**2**) mixture were measured at $T$ = (298.15, 303.15, 308.15, 313.15, and 318.15) K and atmospheric pressure over the entire composition range. Based on the density and viscosity data, the excess properties and viscous flow thermodynamic parameters were calculated, respectively. To obtain the coefficients and to estimate the standard deviations between the experimental and calculated quantities, the excess molar volume ($V_m^E$), the viscosity deviation ($\Delta\eta$), and the excess Gibbs free energies of activation for viscous flow ($\Delta G^{*E}$) were fitted to the Redlich−Kister equation. Furthermore, based on the results of UV−vis, FTIR, and $^1$H NMR spectra, the intermolecular interaction of PEG 200 and DMAPA was discussed. Particularly, a strong intermolecular bonding is formed when the molar ratio of PEG 200 to DMAPA is about 1:2 because of the excess molar volume ($V_m^E$). On that account, a mixture of PEG 200 and DMAPA in a ratio of 1:2 was used for studying $CO_2$ absorption, and a $CO_2$ absorption of about 0.19 g per gram of absorbent was achieved at room temperature and atmosphere.

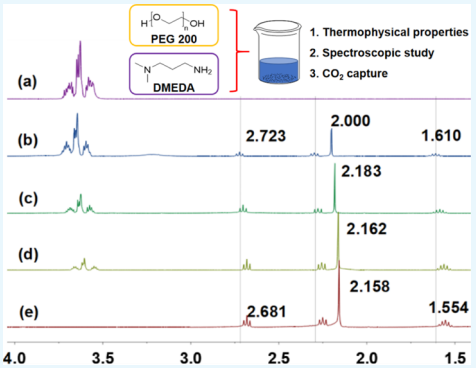


## 1. INTRODUCTION

The extensive use of fossil fuels and the rapid increase of $CO_2$ content in the atmosphere have caused the greenhouse effect and the negative consequences of global climate changes, and this has attracted widespread attention.[1,2] Experts generally deem $CO_2$ capture and utilization (CCU) to be one of the most effective methods to reduce global $CO_2$ emissions.[3,4] Various methods have been proposed to capture $CO_2$, such as solid adsorption,[5,6] membrane separation,[7,8] and organic solvent scrubbing.[9−11] The organic solvent scrubbing method involves either physical or chemical solvents according to the strength of the solvent−solute interaction. Representative amine scrubbing is the most commonly used commercial technology for $CO_2$ capture through chemical absorption.[12,13] However, the loss of amine by volatilization easily causes secondary pollution in the process of $CO_2$ removal. Especially, there are also some shortcomings, such as equipment corrosion, relatively high cost, and serious loss of efficiency. To improve the process of amine absorption of $CO_2$, the selection of a suitable solvent is important. Thus, it is the focus of this study to find an organic solvent that can reduce the volatilization of amine, has better $CO_2$ uptake, and causes less environmental damage. Previous studies[14−17] have shown that addition of certain organic solvents, such as alcohol and ethylene glycol derivatives, to combine with amines, has dramatically reduced the volatilization of amines, and the resulting amine−alcohol binary system showed superior $CO_2$ absorption capacity. Polyethylene glycol 200 (PEG 200) has been widely studied for $CO_2$ absorption because it has many good properties.[18,19] Especially, it has reasonable characteristics to be labeled as a green solvent such as being nonvolatile, noncombustible, nontoxic to humans, animals, and aquatic organisms, and can be biodegraded by bacteria in soil and sewage. These properties make it suitable for replacing the previously used organic auxiliary solvent of alcohol for $CO_2$ capture.

In the course of our study on the capture of $CO_2$,[20] we found that 3-dimethylamino-1-propylamine (DMAPA) can efficiently absorb $CO_2$ through intramolecular proton transfer. However, the problem of high volatility of DMAPA is still difficult to solve. Inspired by $CO_2$ organic binding solutions

Received: February 4, 2021
Accepted: March 12, 2021
Published: March 31, 2021

Table 1. Density Data for the Binary System of PEG 200 (1) + DMAPA (2) as a Function of PEG 200 Mole Fraction ($x_1$) at $T$ = (298.15, 303.15, 308.15, 313.15, and 318.15) K and Atmospheric Pressure[a]

| | $\rho$/(g·cm$^{-3}$) | | | | |
|---|---|---|---|---|---|
| $x_1$ | $T$ = 298.15 K | $T$ = 303.15 K | $T$ = 308.15 K | $T$ = 313.15 K | $T$ = 318.15 K |
| 0.0000 | 0.8098 | 0.8042 | 0.8023 | 0.7949 | 0.7938 |
| 0.0262 | 0.8323 | 0.8296 | 0.8265 | 0.8197 | 0.8216 |
| 0.0537 | 0.8585 | 0.8532 | 0.8476 | 0.8441 | 0.8435 |
| 0.0827 | 0.8807 | 0.8731 | 0.8700 | 0.8677 | 0.8672 |
| 0.1133 | 0.9008 | 0.8973 | 0.8917 | 0.8890 | 0.8879 |
| 0.1455 | 0.9205 | 0.9158 | 0.9119 | 0.9083 | 0.9075 |
| 0.1796 | 0.9394 | 0.9358 | 0.9302 | 0.9278 | 0.9267 |
| 0.2157 | 0.9573 | 0.9522 | 0.9473 | 0.9445 | 0.9434 |
| 0.2541 | 0.9746 | 0.9714 | 0.9664 | 0.9610 | 0.9600 |
| 0.2948 | 0.9907 | 0.9867 | 0.9822 | 0.9784 | 0.9774 |
| 0.3381 | 1.0053 | 1.0012 | 0.9966 | 0.9933 | 0.9922 |
| 0.3844 | 1.0192 | 1.0164 | 1.0116 | 1.0071 | 1.0062 |
| 0.4339 | 1.0328 | 1.0295 | 1.0251 | 1.0215 | 1.0206 |
| 0.4869 | 1.0455 | 1.0417 | 1.0378 | 1.0314 | 1.0308 |
| 0.5438 | 1.0566 | 1.0546 | 1.0497 | 1.0460 | 1.0450 |
| 0.6052 | 1.0690 | 1.0661 | 1.0618 | 1.0574 | 1.0560 |
| 0.6714 | 1.0791 | 1.0767 | 1.0718 | 1.0684 | 1.0659 |
| 0.7433 | 1.0900 | 1.0860 | 1.0811 | 1.0788 | 1.0781 |
| 0.8214 | 1.1001 | 1.0958 | 1.0926 | 1.0851 | 1.0832 |
| 0.9066 | 1.1064 | 1.1043 | 1.1013 | 1.0975 | 1.0964 |
| 1.0000 | 1.1213 | 1.1175 | 1.1139 | 1.1090 | 1.1057 |

[a]Standard uncertainties $u$ for each variable are $u$ ($T$) = 0.01 K, $u$ ($p$) = ± 5%, and $u$ ($x_1$) = 0.0001 and the combined expanded uncertainty is $u_c$ ($\rho$) = ± 0.02%, with a 0.95 level of confidence ($k \approx 2$).

(superbase plus butanol),[21] we propose to prepare a hydrogen bond-mixture solution of PEG 200 plus DMAPA for $CO_2$ absorption. The systematic study of $CO_2$ absorption processes for the PEG 200 (**1**) + DMAPA (**2**) system includes the following three steps: (1) determining the density, viscosity, and excess properties of the PEG 200 (**1**) + DMAPA (**2**) mixture, (2) obtaining the gas−liquid equilibrium data for the gas mixture of $CO_2$ + $N_2$ at various concentrations of PEG 200 (**1**) + DMAPA (**2**), and (3) determining the spectral properties of the PEG 200 (**1**) + DMAPA (**2**) + $CO_2$ system. To the best of our knowledge, studies on the thermodynamic properties of the binary system of PEG 200 (**1**) + DMAPA (**2**), such as density ($\rho$), viscosity ($\eta$), and excess properties, over a wide experimental temperature range are very lacking. Herein, the present work mainly focuses on investigating the density and viscosity data at $T$ = (298.15, 303.15, 308.15, 313.15, and 318.15) K for the whole composition range. Based on the above experimental results, the excess molar volume ($V_m^E$), viscosity deviation ($\Delta\eta$), and the excess Gibbs free energies of activation for viscous flow ($\Delta G^{*E}$) were calculated. According to the results of excess properties, the $CO_2$ uptake of the PEG 200 (**1**) + DMAPA (**2**) system was also studied. These results can be used to obtain important basic data for potential industrial applications. Furthermore, the possible intermolecular interaction of PEG 200 with DMAPA was also investigated using UV−vis, FTIR, and $^1$H NMR spectroscopic techniques.

## 2. RESULTS AND DISCUSSION

**2.1. Density and Viscosity.** The density of PEG 200 (**1**) + DMAPA (**2**) mixtures with different compositions at atmospheric pressure and $T$ = (298.15, 303.15, 308.15, 313.15, and 318.15) K was determined. The results are shown in Table 1 and Figure 1, where the mole fraction of PEG 200 is expressed by $x_1$.

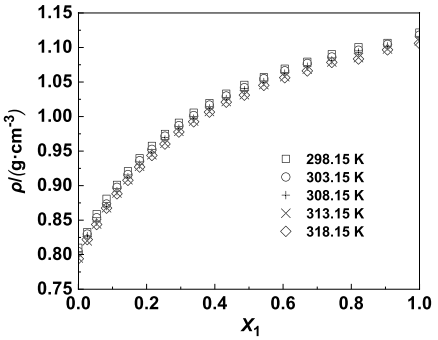


**Figure 1.** Changes in experimental densities with molar fraction for PEG 200 (**1**) + DMAPA (**2**) at $T$ = (298.15, 303.15, 308.15, 313.15, and 318.15) K.

It can be seen from Figure 1 that the density of mixtures increases with the increase of the mole fraction of PEG 200 at the same temperature. In the same sample, the density of the mixtures decreases with the increase of temperature. The density of the binary solution can be calculated using eq 1)[22]

$$\rho_{cal.} = \frac{x_1M_1 + x_2M_2}{V_1 + V_2 + x_1x_2\sum_{i=0}^{n} A_i(2x_1 - 1)^i} \quad (1)$$

where $x_1$, $M_1$ and $x_2$, $M_2$ represent the molar fraction and relative molecular weight of pure PEG 200 and pure DMAPA, respectively. $V_1$ and $V_2$ are the molar volumes of pure PEG 200 and DMAPA, respectively. $A_i$ represents the fitting parameters.

The average absolute deviation was calculated using eq 2[22]



https://doi.org/10.1021/acsomega.1c00667
ACS Omega 2021, 6, 9898−9909

$$\mathrm{AAD}\% = \frac{\sum |100 \times (Y_{\mathrm{exp.}} - Y_{\mathrm{cal.}})/Y_{\mathrm{exp.}}|}{n} \quad (2)$$

where $Y_{\mathrm{exp.}}$ is the experimental density value. $Y_{\mathrm{cal.}}$ is the calculated density value. $n$ is the number of experiments. The relative deviation of density of the PEG 200 (**1**) + DMAPA (**2**) mixture is within ±0.002 and is plotted in Figure 2.

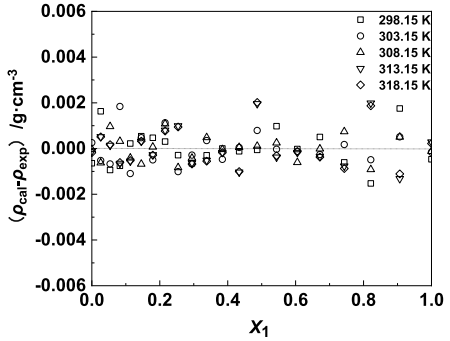


**Figure 2.** Difference in density ($\rho_{\mathrm{cal.}} - \rho_{\mathrm{exp.}}$) values between the experimental data and calculated values for the binary system of PEG 200 (**1**) + DMAPA (**2**) at $T$ = (298.15, 303.15, 308.15, 313.15, and 318.15) K.

The viscosity of the PEG 200 (**1**) + DMAPA (**2**) mixture at $T$ = (298.15, 303.15, 308.15, 313.15, and 318.15) K was measured with an Ubbelohde viscometer. The viscosity data are listed in Table 2 and plotted in Figure 3. From Figure 3, one can find that the viscosity decreases gradually with the increase of temperature. This phenomenon indicates that the molecular energy of the binary system solution tends to increase with the increase of temperature. With the increase of the mole fraction of PEG 200, the viscosity of mixtures increases first and then decreases at the same temperature. When the mole fraction of PEG 200 is greater than 0.66, the viscosity increases more slowly. Particularly, when the mole fraction of PEG 200 is 0.8214, the viscosity reaches the maximum value and then begins to decrease.

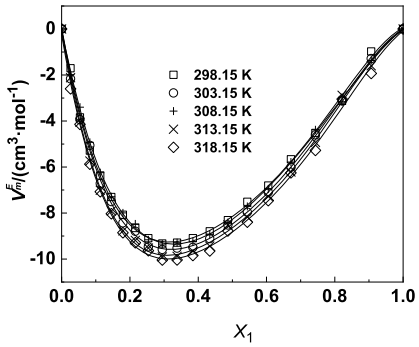


**Figure 3.** excess molar volume ($V_m^E$) with the mole fraction for the binary system of PEG 200 (**1**) + DMAPA (**2**) at $T$ = (298.15, 303.15, 308.15, 313.15, and 318.15) K. The symbols represent the experimental values, and the solid curves represent the calculated values.

The viscosity can be calculated using eq 3[23−25]

$$\eta_{\mathrm{cal.}} = x_1\eta_1 + x_2\eta_2 + x_1x_2\sum_{i=0}^{n} A_i(2x_1 - 1)^i \quad (3)$$

where $x_1$ and $x_2$ denote the mole fractions of PEG 200 and DMAPA, respectively. $\eta$ is the viscosity of mixtures, and $\eta_1$ and $\eta_2$ represent the viscosity values of pure PEG 200 and DMAPA, respectively. The relative deviation of viscosity between the experimental value and the calculated value is

**Table 2. Viscosity Data for the Binary System of PEG 200 (1) + DMAPA (2) as a Function of PEG 200 Mole Fraction ($x_1$) at $T$ = (298.15, 303.15, 308.15, 313.15, and 318.15) K and Atmospheric Pressure**[a]

| | $\eta$/(mPa·s) | | | | |
|---|---|---|---|---|---|
| $x_1$ | $T$ = 298.15 K | $T$ = 303.15 K | $T$ = 308.15 K | $T$ = 313.15 K | $T$ = 318.15 K |
| 0.0000 | 1.06 | 1.04 | 1.02 | 1.00 | 0.99 |
| 0.0262 | 1.66 | 1.58 | 1.54 | 1.53 | 1.50 |
| 0.0537 | 2.28 | 2.13 | 2.02 | 1.98 | 1.96 |
| 0.0827 | 3.30 | 3.03 | 2.84 | 2.73 | 2.66 |
| 0.1133 | 4.67 | 4.23 | 3.89 | 3.69 | 3.57 |
| 0.1455 | 6.58 | 5.93 | 5.34 | 4.96 | 4.71 |
| 0.1796 | 9.14 | 8.01 | 7.11 | 6.54 | 6.15 |
| 0.2157 | 12.34 | 10.66 | 9.24 | 8.42 | 7.80 |
| 0.2541 | 16.22 | 13.85 | 11.88 | 10.78 | 9.79 |
| 0.2948 | 20.78 | 17.68 | 15.29 | 13.26 | 12.16 |
| 0.3381 | 25.74 | 21.52 | 17.98 | 15.93 | 14.35 |
| 0.3844 | 30.91 | 25.71 | 21.34 | 18.79 | 16.66 |
| 0.4339 | 36.11 | 30.09 | 24.68 | 21.69 | 19.20 |
| 0.4869 | 40.91 | 33.78 | 27.87 | 24.36 | 21.38 |
| 0.5438 | 45.25 | 37.32 | 30.76 | 26.68 | 23.44 |
| 0.6052 | 49.05 | 40.19 | 33.04 | 28.96 | 25.33 |
| 0.6714 | 51.42 | 42.45 | 35.55 | 30.51 | 26.73 |
| 0.7433 | 53.61 | 44.18 | 36.37 | 31.81 | 27.79 |
| 0.8214 | 55.52 | 45.63 | 37.25 | 32.74 | 28.75 |
| 0.9066 | 55.51 | 46.04 | 37.84 | 33.25 | 29.67 |
| 1.0000 | 54.56 | 45.65 | 37.59 | 30.60 | 27.29 |

[a]Standard uncertainties $u$ for each variables are $u$ ($T$) = ± 0.01 K, $u$ ($p$) = 5%, and $u$ ($x_1$) = 0.0001, and the combined expanded uncertainty is $u_c$ ($\eta$) = ± 3%, with a 0.95 level of confidence ($k \approx 2$).



https://doi.org/10.1021/acsomega.1c00667
ACS Omega 2021, 6, 9898−9909

plotted in Figure 4. It was found that the relative deviation of viscosity data is within ±0.65.

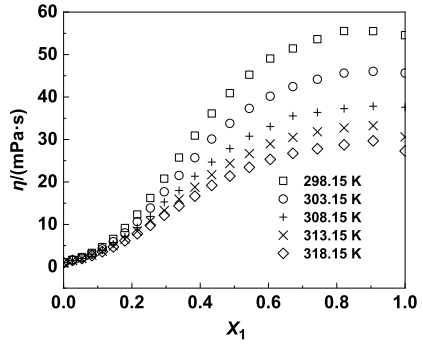


**Figure 4.** Changes in experimental viscosities with the molar fraction for PEG 200 (**1**) + DMAPA (**2**) at $T$ = (298.15, 303.15, 308.15, 313.15, and 318.15) K.

**2.2. Excess Property.** The excess molar volume ($V_m^E$) of the binary system can be calculated using eq 4[23−25]

$$V_m^E = (x_1M_1 + x_2M_2)/\rho - (x_1M_1/\rho_1 + x_2M_2/\rho_2) \quad (4)$$

where $\rho$ represents the density of the mixtures; $x_1$, $\rho_1$, and $M_1$ and $x_2$, $\rho_2$, and $M_2$ are the mole fraction, density, and relative molecular weight of pure PEG 200 and DMAPA, respectively.

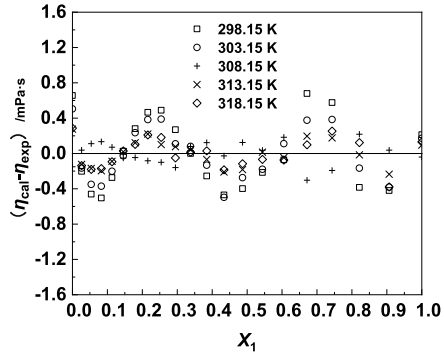


**Figure 5.** Figure 5Difference in the viscosity deviation ($\eta_{cal.} - \eta_{exp.}$) values between the experimental data and calculated values for the binary system of PEG 200 (**1**) + DMAPA (**2**) at $T$ = (298.15, 303.15, 308.15, 313.15, and 318.15) K.

Figure 5 and Table 3 show that the $V_m^E$ in all composition ranges is negative at the experimental temperatures. That is, the volume of the mixed solution is less than the sum of the volumes before the two liquids are mixed. With the same composition, the $V_m^E$ increases with the increase of temperature. The $V_m^E$ of the binary solution mixture is mainly related to the chemical action, physical properties, and structural properties of the components. The negative $V_m^E$ values of mixtures indicate that there is a certain interaction force between PEG 200 and DMAPA, which makes the intermolecular distance smaller and the volume to shrink. Particularly, when the molar ratio of DMAPA and PEG 200 is about 2:1, the $V_m^E$ is the lowest, meaning that the intermolecular bonding is the strongest at this concentration.

$$\Delta\eta = \eta - (x_1\eta_1 + x_2\eta_2) \quad (5)$$

where $\eta$ represents the viscosity of the PEG 200 (**1**) + DMAPA (**2**) system. $\eta_1$ and $\eta_2$ represent the viscosity of pure PEG 200 and DMAPA, respectively. $x_1$ and $x_2$ represent the mole fraction of PEG 200 and DMAPA, respectively. Figure 6 and Table 4 show the dependence of viscosity deviations on composition and temperature. It can be seen from each $\Delta\eta$ curve of the PEG 200 (**1**) + DMAPA (**2**) mixture that the value of $\Delta\eta$ is not always negative but also shows a positive maximum and negative minimum at around $x_1 \approx 0.6067$ and $x_1 \approx 0.1158$, respectively. The curves become more and more flat, and the absolute values decrease at elevated temperatures.

The excess Gibbs free energies of activation for viscous flow ($\Delta G^{*E}$) values were calculated from the viscosity data using eq 6[26]

$$\Delta G^{*E} = RT[\ln(\eta V) - x_1\ln(\eta_1 V_1) - x_2\ln(\eta_2 V_2)] \quad (6)$$

where R is the general constant of the gas, $T$ is the absolute temperature, $V$, $V_1$, and $V_2$ are the molar volumes of the binary mixtures, pure PEG 200, and DMAPA, respectively, $\eta$, $\eta_1$, and $\eta_2$ are the absolute viscosity of the binary mixtures, pure PEG 200, and DMAPA, respectively. The values of $\Delta G^{*E}$ are given in Table 5 and are plotted in Figure 7.

As shown in Figure 7, the values of $\Delta G^{*E}$ are all positive in the whole concentration range. $\Delta G^{*E}$ can be used as a reliable standard to detect the interaction between different molecules.[27] Here, the results of $\Delta G^{*E}$ show that there is an interaction between PEG 200 and DMAPA.

The polynomial regression values of $V_m^E$, $\Delta\eta$, and $\Delta G^{*E}$ were calculated using the Redlich Kister eq 7

$$Q = x_1(1 - x_1)\sum_{i=0}^{n} A_i(2x_1 - 1)^i \quad (7)$$

where $Q$ represents $V_m^E$, $\Delta\eta$, and $\Delta G^{*E}$. $x_1$ represents the mole fraction of PEG 200 and $A_i$ is the polynomial regression coefficient. In order to study the fitting efficiency of $V_m^E$, $\Delta\eta$, and $\Delta G^{*E}$, the standard deviations between the calculated value and the experimental value were acquired from eq 8

$$\sigma = \left[\sum_{i=1}^{N} (Z^E_{cal.,i} - Z^E_{exp.,i})^2/(N - m)\right]^{1/2} \quad (8)$$

where $Z$ represents $V_m^E$, $\Delta\eta$, or $\Delta G^{*E}$, and $N$ and $m$ are the number of experimental points and the number of parameters retained in the respective equations. The calculated values $A_i$ and $\sigma$ and the fitting degree($R^2$) are shown in Table 6.

The apparent molar volumes $V_{\varphi,1}$ and $V_{\varphi,2}$ of the binary mixture were obtained from eqs 9 and 10,[28] and the results are listed in Table 7.

$$V_{\varphi,1} = \frac{x_2M_2}{x_1} \times \frac{\rho_2 - \rho_m}{\rho_2\rho_m} + \frac{M_1}{\rho_m} \quad (9)$$

$$V_{\varphi,2} = \frac{x_1M_1}{x_2} \times \frac{\rho_1 - \rho_m}{\rho_1\rho_m} + \frac{M_2}{\rho_m} \quad (10)$$

where $\rho_m$ is the density of the mixture, and $x_1$, $\rho_1$, and $M_1$ and $x_2$, $\rho_2$, and $M_2$ are the mole fraction, density value, and relative molecular weight of pure PEG 200 and DMAPA, respectively. Table 9 shows that the apparent molar volumes of binary solutions $V_{\varphi,1}$ and $V_{\varphi,2}$ increase with the increase of temperature at the same composition. At a certain temperature, the apparent molar volume of the binary solution $V_{\varphi,1}$


https://doi.org/10.1021/acsomega.1c00667
ACS Omega 2021, 6, 9898−9909

Table 3. Excess Molar Volumes ($V_m^E$) for the Binary System of PEG 200 (1) + DMAPA (2) at $T$ = (298.15, 303.15, 308.15, 313.15, and 318.15) K[a]

| | $V_m^E/(cm^3 \cdot mol^{-1})$ | | | | |
|---|---|---|---|---|---|
| $x_1$ | $T$ = 298.15 K | $T$ = 303.15 K | $T$ = 308.15 K | $T$ = 313.15 K | $T$ = 318.15 K |
| 0.0000 | 0.0000 | 0.0000 | 0.0000 | 0.0000 | 0.0000 |
| 0.0262 | −1.7083 | −2.1642 | −1.9843 | −2.1180 | −2.6013 |
| 0.0537 | −3.8424 | −3.9372 | −3.3991 | −4.0538 | −4.1461 |
| 0.0827 | −5.2871 | −5.0583 | −4.9254 | −5.7380 | −5.8736 |
| 0.1133 | −6.3670 | −6.7161 | −6.2447 | −7.0076 | −7.0726 |
| 0.1455 | −7.3049 | −7.5030 | −7.2899 | −7.9086 | −8.0298 |
| 0.1796 | −8.0756 | −8.4267 | −7.9954 | −8.7758 | −8.8577 |
| 0.2157 | −8.6536 | −8.7912 | −8.4734 | −9.1898 | −9.2909 |
| 0.2541 | −9.0955 | −9.4720 | −9.1634 | −9.5216 | −9.6386 |
| 0.2948 | −9.3248 | −9.5820 | −9.3503 | −9.9103 | −10.0429 |
| 0.3381 | −9.2877 | −9.5269 | −9.2876 | −9.8840 | −10.0395 |
| 0.3844 | −9.0934 | −9.4964 | −9.2356 | −9.6581 | −9.8447 |
| 0.4339 | −8.7954 | −9.1128 | −8.9158 | −9.4385 | −9.6484 |
| 0.4869 | −8.3083 | −8.5222 | −8.4152 | −8.5180 | −8.7788 |
| 0.5438 | −7.5121 | −7.9618 | −7.7111 | −8.1737 | −8.3938 |
| 0.6052 | −6.8057 | −7.0975 | −6.9522 | −7.2794 | −7.4595 |
| 0.6714 | −5.6654 | −6.0137 | −5.7823 | −6.2147 | −6.2528 |
| 0.7433 | −4.5201 | −4.6007 | −4.3817 | −4.9268 | −5.2759 |
| 0.8214 | −3.1235 | −3.1243 | −3.1621 | −2.8816 | −3.0499 |
| 0.9066 | −0.9768 | −1.2871 | −1.3667 | −1.5997 | −1.9304 |
| 1.0000 | 0.0000 | 0.0000 | 0.0000 | 0.0000 | 0.0000 |

[a]The viscosity deviation ($\Delta\eta$) of the binary system was calculated according to eq 5).[23−25]

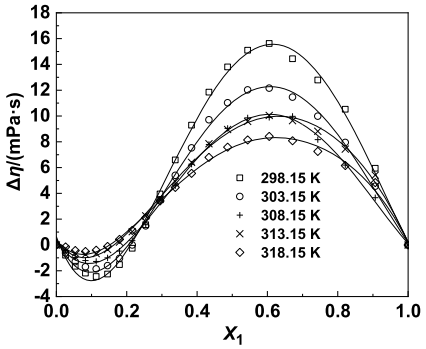


**Figure 6.** Viscosity deviation ($\Delta\eta$) with the mole fraction for the binary system of PEG 200 (**1**) + DMAPA (**2**) $T$ = (298.15, 303.15, 308.15, 313.15, and 318.15) K. The symbols represent experimental values, and the solid curves represent the values calculated from eq 7.

increases and that of $V_{\varphi,2}$ decreases with the increase of the mole fraction of PEG 200.

The partial molar volume of the mixed solution was calculated using equation 11 and 12[28]

$$\bar{V}_1 = V_m^E + V_1 + (1 - x_1)\left(\frac{\partial V_m^E}{\partial x_1}\right)_{P,T} \quad (11)$$

$$\bar{V}_2 = V_m^E + V_2 - x_1\left(\frac{\partial V_m^E}{\partial x_1}\right)_{P,T} \quad (12)$$

where $V_1$and $V_2$ are the molar volumes of the pure components and $V_m^E$ is the excess molar volume of the mixture. The calculated data are listed in Table 8 The partial molar volumes of $\bar{V}_1$ and $\bar{V}_2$ increase with the increase of the mole fraction of PEG 200, while $\bar{V}_1$ and $\bar{V}_2$ do not change significantly with temperatures.

**2.3. Thermodynamic Parameters.** The $V_m^E$ of the PEG 200 (**1**) + DMAPA (**2**) mixture is negative, which proves that there is an interaction between PEG 200 and DMAPA. This intermolecular interaction can also be explained by the thermodynamics of viscous fluids. To obtain the kinematic viscosity of the PEG 200 (**1**) + DMAPA (**2**) system, the thermodynamic parameters of the viscous fluid of the PEG 200 (**1**) + DMAPA (**2**) system were calculated, including the activation enthalpy $\Delta H^*$, activation entropy $\Delta S^*$, and activation Gibbs free energy $\Delta G^*$ using eqs 13 and 14[29]

$$\Delta G^* = \Delta H^* - T\Delta S^* \quad (13)$$

$$\upsilon = \frac{hN_A}{M}\exp\left(\frac{\Delta G^*}{RT}\right) \quad (14)$$

where $\upsilon$, $h$, $N_A$, $M$, and R, respectively, represent the kinematic viscosity, Planck constant, Avogadro constant, average molar mass, and molar gas constant of the binary system. From 13 and 14, the following formula can be obtained:

$$R\ln\left(\upsilon\frac{M}{hN_A}\right) = \frac{\Delta H^*}{T} - \Delta S^* \quad (15)$$

$R\ln(\nu M/hN_A)$ on the left side of eq 15 was found to be in a linear relationship with $1/T$ on the right side, when a plot was constructed by taking $1/T$ as the abscissa and $R\ln(\nu M/hN_A)$ as the ordinate. The fitting results are shown in Figure 8. The slope is the $\Delta H^*$ value and the intercept is the $-\Delta S^*$ value, and the results are shown in Table 9. The activation Gibbs free energy $\Delta G^*$ can also be calculated using eq 13, and the results obtained are shown in Table 9 and plotted in Figure 9.

It was found from Table 9 that the value of $\Delta G^*$ over the range of components is positive at measured temperatures and $\Delta H^*$ increases from 1.51 to 27.63 kJ·mol$^{-1}$·K$^{-1}$. The results


https://doi.org/10.1021/acsomega.1c00667
ACS Omega 2021, 6, 9898−9909

Table 4. Viscosity Deviation ($\Delta\eta$) for the Binary System of PEG 200 (1) + DMAPA (2) at $T$ = (298.15, 303.15, 308.15, 313.15, and 318.15) K

| | $\Delta\eta$/(mPa·s) | | | | |
|---|---|---|---|---|---|
| $x_1$ | $T$ = 298.15 K | $T$ = 303.15 K | $T$ = 308.15 K | $T$ = 313.15 K | $T$ = 318.15 K |
| 0.0000 | 0.00 | 0.00 | 0.00 | 0.00 | 0.00 |
| 0.0262 | −0.80 | −0.62 | −0.44 | −0.28 | −0.15 |
| 0.0537 | −1.65 | −1.30 | −0.97 | −0.63 | −0.43 |
| 0.0827 | −2.18 | −1.70 | −1.21 | −0.72 | −0.51 |
| 0.1133 | −2.45 | −1.86 | −1.28 | −0.67 | −0.41 |
| 0.1455 | −2.26 | −1.60 | −1.00 | −0.35 | −0.12 |
| 0.1796 | −1.52 | −1.04 | −0.48 | 0.22 | 0.43 |
| 0.2157 | −0.26 | 0.00 | 0.33 | 1.03 | 1.13 |
| 0.2541 | 1.57 | 1.48 | 1.57 | 2.26 | 2.12 |
| 0.2948 | 3.95 | 3.49 | 3.49 | 3.54 | 3.41 |
| 0.3381 | 6.59 | 5.40 | 4.59 | 4.92 | 4.46 |
| 0.3844 | 9.29 | 7.53 | 6.26 | 6.41 | 5.55 |
| 0.4339 | 11.85 | 9.70 | 7.80 | 7.85 | 6.79 |
| 0.4869 | 13.80 | 11.02 | 9.04 | 8.95 | 7.58 |
| 0.5438 | 15.10 | 12.02 | 9.85 | 9.58 | 8.14 |
| 0.6052 | 15.62 | 12.16 | 9.89 | 10.04 | 8.42 |
| 0.6714 | 14.44 | 11.46 | 9.97 | 9.63 | 8.08 |
| 0.7433 | 12.78 | 9.98 | 8.17 | 8.81 | 7.26 |
| 0.8214 | 10.52 | 7.95 | 6.19 | 7.43 | 6.16 |
| 0.9066 | 5.95 | 4.56 | 3.66 | 5.42 | 4.84 |
| 1.0000 | 0.00 | 0.00 | 0.00 | 0.00 | 0.00 |

Table 5. Excess Gibbs Free Energy of Activation of Viscous Flow ($\Delta G^{*E}$) for the Binary System of PEG (1) + DMAPA (2) at $T$ = (298.15, 303.15, 308.15, 313.15, and 318.15) K

| | $\Delta G^{*E}$/(kJ·mol$^{-1}$) | | | | |
|---|---|---|---|---|---|
| $x_1$ | $T$ = 298.15 K | $T$ = 303.15 K | $T$ = 308.15 K | $T$ = 313.15 K | $T$ = 318.15 K |
| 0.0000 | 0.00 | 0.00 | 0.00 | 0.00 | 0.00 |
| 0.0262 | 0.84 | 0.78 | 0.78 | 0.77 | 0.86 |
| 0.0537 | 1.31 | 1.24 | 1.19 | 1.19 | 1.27 |
| 0.0827 | 1.92 | 1.83 | 1.77 | 1.76 | 1.77 |
| 0.1133 | 2.47 | 2.35 | 2.27 | 2.25 | 2.26 |
| 0.1455 | 3.00 | 2.88 | 2.77 | 2.73 | 2.69 |
| 0.1796 | 3.47 | 3.30 | 3.18 | 3.13 | 3.09 |
| 0.2157 | 3.85 | 3.68 | 3.52 | 3.47 | 3.40 |
| 0.2541 | 4.15 | 3.96 | 3.80 | 3.77 | 3.67 |
| 0.2948 | 4.37 | 4.19 | 4.07 | 3.94 | 3.88 |
| 0.3381 | 4.48 | 4.28 | 4.09 | 4.04 | 3.94 |
| 0.3844 | 4.49 | 4.29 | 4.11 | 4.07 | 3.94 |
| 0.4339 | 4.40 | 4.23 | 4.03 | 4.01 | 3.89 |
| 0.4869 | 4.20 | 4.03 | 3.87 | 3.86 | 3.73 |
| 0.5438 | 3.91 | 3.75 | 3.61 | 3.60 | 3.48 |
| 0.6052 | 3.52 | 3.36 | 3.24 | 3.28 | 3.17 |
| 0.6714 | 3.01 | 2.89 | 2.83 | 2.85 | 2.75 |
| 0.7433 | 2.43 | 2.32 | 2.25 | 2.33 | 2.24 |
| 0.8214 | 1.76 | 1.68 | 1.60 | 1.74 | 1.68 |
| 0.9066 | 0.95 | 0.91 | 0.87 | 1.03 | 1.02 |
| 1.0000 | 0.00 | 0.00 | 0.00 | 0.00 | 0.00 |

indicate that the viscous flow in pure DMAPA is easier than that in pure PEG 200 or the binary solution. At the same time, $\Delta S^*$ increases from −215.52 to −163.61 J·mol$^{-1}$·K$^{-1}$ with the increase of the mole fraction of PEG 200. The negative $\Delta S^*$ indicates that the self-association binding force of PEG 200 and DMAPA is stronger than that of DMAPA alone.

**2.4. Spectral Properties.** *2.4.1. UV−Vis Spectra.* The preceding results may be related to the hydrogen bond and interaction between PEG 200 and DMAPA. The UV−vis spectra of the PEG 200 (**1**) + DMAPA (**2**) mixture were measured and are shown in Figure 10. PEG 200 was used as a reference solvent. The absorption peak of DMAPA was found at about 234 nm, which is attributed to N electrons undergoing the $n \rightarrow \sigma^*$ electron transition. The peak red-shifted from 234 to 237 nm with the increase of the DMAPA concentration. This phenomenon is mainly due to the self-association hydrogen bond between PEG 200 molecules was



https://doi.org/10.1021/acsomega.1c00667
ACS Omega 2021, 6, 9898−9909

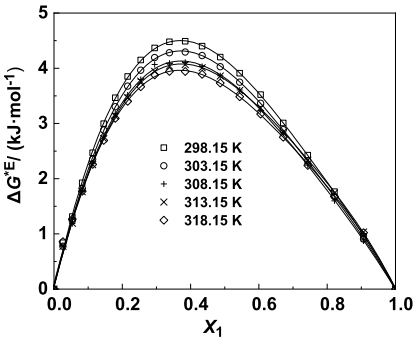


**Figure 7.** Excess Gibbs free energies of activation for the viscous flow ($\Delta G^{*E}$) with the mole fraction for the binary system of PEG 200 (**1**) + DMAPA (**2**) at $T$ = (298.15, 303.15, 308.15, 313.15, and 318.15) K. The symbols represent experimental values, and the solid curves represent the values calculated from eq 7.

broken, and the new hydrogen bond was formed between PEG 200 and DMAPA through the formation of $(CH_3)_2N\cdots HOCH_2CH-O-$ and $H_2N\cdots HOCH_2CH-O$-. Particularly, the ability of DMAPA molecules to form a hydrogen bond with PEG 200 molecules was reinforced with the increase of the DMAPA concentration, which will make the nitrogen atom in DMAPA molecules interact more easily with hydroxyl on PEG 200, leading to the red shift of the absorption peak.

*2.4.2. FTIR Spectra.* To further study the interaction between DMAPA and PEG 200, the FTIR spectra of PEG 200, DMAPA, and the binary system of PEG 200 (**1**) + DMAPA (**2**) at various concentrations were obtained. In the FTIR spectra shown in Figure 11, the stretching vibration peak of the O−H bond in PEG 200 molecules appears at 3422 $cm^{-1}$.[30] Interestingly, the absorption peak moves to a low wavenumber of 3356 $cm^{-1}$ with an increase of the DMAPA concentration; meanwhile, the bending vibration band of the hydroxyl group in PEG 200 moved from 1104 $cm^{-1}$ to a lower frequency of 1100 $cm^{-1}$ with the increase of the DMAPA concentration. These results suggest that the intermolecular hydrogen bonds in PEG 200 are broken gradually, and new hydrogen bonds are formed. The absorption band of hydroxyl groups in PEG 200 moves to a lower frequency, which is due to the vibrational properties of hydroxyl groups in PEG 200, further indicating the hydrogen bonding and interaction of the hydroxyl hydrogen atoms in PEG 200 with nitrogen atoms in DMAPA.

*2.4.3. $^1$H NMR Spectra.* The $^1$H NMR spectra of PEG 200, DMAPA, and the binary system of PEG 200 (**1**) + DMAPA (**2**) with various concentrations were also compared. Figure 12 shows that the chemical displacement of methyl hydrogen in DMAPA is 2.158 ppm. With the increase of the PEG 200 concentration, the chemical displacement gradually moves to a low field of 2.000 ppm; meanwhile, the chemical shifts of other methylene groups in DMAPA also move to the lower field. The fact is that the electron cloud density of protons on DMAPA becomes thinner due to hydrogen bonding interactions between DMAPA and PEG 200. The most reasonable form of hydrogen bonding was proposed as the formation of $(CH_3)_2N\cdots HOCH_2CH-O-$ and $H_2N\cdots HOCH_2CH-O-$. The results are in well accordance with the FTIR and UV−vis results.

**2.5. $CO_2$ Absorption.** Based on the above experimental results, the PEG 200 plus DMAPA mixture was used to measure $CO_2$ absorption. Figure 13a shows the relationship between $CO_2$ uptake and time at room temperature and atmospheric pressure. The absorption equilibrium of PEG 200 + DMAPA (1:1 mole ratio), PEG 200 + DMAPA (1:2), and PEG 200 + DMAPA (2:1) was all achieved within 45 min. In contrast, the absorption capacity of $CO_2$ of PEG 200 + DMAPA (1:2) is quite large, reaching 0.19 g $CO_2$ per gram solvent. Interestingly, when the molar ratio of PEG 200 and DMAPA is 1:2, the intermolecular bonding is the most strongest based on the results obtained for $V_m^E$ of the mixture. This intermolecular hydrogen bonding can reduce the volatility of amines, which will be further discussed later. Considering the importance of $CO_2$ removal efficiency in practical industrial processes, we investigated low-concentration $CO_2$ removal under environmental conditions. As shown in Figure 13b, it was found that $CO_2$ was completely removed in the first 40 min using PEG 200 + DMAPA (1:2) as the absorbent, then the removal efficiency was reduced, and the final absorption reaches saturation in about 60 min.

## 3. CONCLUSIONS

In summary, the density and viscosity of the PEG 200 (**1**) + DMAPA (**2**) binary solution in the whole concentration range

**Table 6. Coefficients of the Redlich−Kister Equation and Standard Deviations for $V_m^E$/($cm^3$·$mol^{-1}$), $\Delta\eta$/(mPa·s), and $\Delta G^{*E}$/(kJ·$mol^{-1}$) for the Binary System of PEG 200 (1) + DMAPA (2) at Different Temperatures; $R^2$ is the Degree of Fitting**

| $T$/(K) | property | $A_3$ | $A_2$ | $A_1$ | $A_0$ | $\sigma$ | $R^2$ |
|---|---|---|---|---|---|---|---|
| | $V_m^E$/($cm^3$·$mol^{-1}$) | −32.8245 | 21.1379 | −12.4724 | 16.3136 | 0.1487 | 0.9981 |
| 298.15 | $\Delta\eta$/(mPa·s) | 53.57 | 60.38 | −63.77 | 3.84 | 0.72 | 0.9953 |
| | $\Delta G^{*E}$/(kJ·$mol^{-1}$) | 16.52 | −9.70 | 2.45 | 2.28 | 0.06 | 0.9993 |
| | $V_m^E$/($cm^3$·$mol^{-1}$) | −33.7457 | 21.6664 | −11.7893 | 15.0121 | 0.1296 | 0.9987 |
| 303.15 | $\Delta\eta$/(mPa·s) | 42.93 | 45.03 | −52.19 | 4.16 | 0.55 | 0.9958 |
| | $\Delta G^{*E}$/(kJ·$mol^{-1}$) | 15.86 | −9.33 | 2.21 | 2.21 | 0.05 | 0.9994 |
| | $V_m^E$/($cm^3$·$mol^{-1}$) | −33.0189 | 22.2396 | −10.7541 | 9.7849 | 0.0948 | 0.9991 |
| 308.15 | $\Delta\eta$/(mPa·s) | 35.80 | 36.07 | −40.87 | −0.49 | 0.35 | 0.9969 |
| | $\Delta G^{*E}$/(kJ·$mol^{-1}$) | 15.24 | −8.66 | 2.20 | 1.46 | 0.05 | 0.9989 |
| | $V_m^E$/($cm^3$·$mol^{-1}$) | −34.4147 | 21.8592 | −14.3372 | 18.8922 | 0.1476 | 0.9980 |
| 313.15 | $\Delta\eta$/(mPa·s) | 34.45 | 32.45 | −22.57 | 16.16 | 0.45 | 0.9953 |
| | $\Delta G^{*E}$/(kJ·$mol^{-1}$) | 15.07 | −8.00 | 3.17 | 2.27 | 0.06 | 0.9992 |
| | $V_m^E$/($cm^3$·$mol^{-1}$) | −34.6386 | 21.4404 | −14.8585 | 16.5294 | 0.2882 | 0.9963 |
| 318.15 | $\Delta\eta$/(mPa·s) | 29.11 | 24.10 | −17.83 | 18.60 | 0.44 | 0.9931 |
| | $\Delta G^{*E}$/(kJ·$mol^{-1}$) | 14.47 | −7.79 | 3.44 | 1.75 | 0.10 | 0.9983 |


https://doi.org/10.1021/acsomega.1c00667
ACS Omega 2021, 6, 9898−9909

Table 7. Apparent Molar Volumes $V_{\varphi,1}$ and $V_{\varphi,2}$ for the Binary System of PEG 200 and DMAPA at $T$ = (298.15, 303.15, 308.15, 313.15, and 318.15) K

| | $V_{\varphi,1}$(PEG)/(cm$^3$·mol$^{-1}$) | | | | | $V_{\varphi,2}$(DMAPA)/(cm$^3$·mol$^{-1}$) | | | | |
|---|---|---|---|---|---|---|---|---|---|---|
| $x_1$ | $T$/K = 298.15 | 303.15 | 308.15 | 313.15 | 318.15 | $T$/K = 298.15 | 303.15 | 308.15 | 313.15 | 318.15 |
| 0.0000 | | | | | | 126.19 | 127.06 | 127.35 | 128.54 | 128.72 |
| 0.0262 | 113.12 | 128.99 | 147.16 | 187.20 | 175.73 | 124.42 | 124.85 | 125.33 | 126.41 | 126.10 |
| 0.0537 | 106.83 | 121.15 | 136.83 | 146.44 | 148.31 | 122.10 | 122.91 | 123.80 | 124.35 | 124.45 |
| 0.0827 | 114.44 | 127.55 | 132.93 | 137.13 | 137.95 | 120.38 | 121.56 | 122.05 | 122.43 | 122.50 |
| 0.1133 | 122.15 | 126.55 | 133.55 | 136.94 | 138.26 | 118.95 | 119.51 | 120.40 | 120.84 | 121.01 |
| 0.1455 | 128.17 | 132.57 | 136.30 | 139.85 | 140.57 | 117.56 | 118.31 | 118.95 | 119.55 | 119.67 |
| 0.1796 | 133.41 | 136.07 | 140.37 | 142.26 | 143.14 | 116.24 | 116.83 | 117.77 | 118.18 | 118.37 |
| 0.2157 | 138.25 | 141.42 | 144.52 | 146.32 | 147.02 | 115.03 | 115.90 | 116.75 | 117.25 | 117.44 |
| 0.2541 | 142.56 | 144.27 | 146.91 | 149.79 | 150.38 | 113.84 | 114.42 | 115.32 | 116.30 | 116.50 |
| 0.2948 | 146.73 | 148.57 | 150.62 | 152.37 | 152.87 | 112.77 | 113.54 | 114.40 | 115.13 | 115.34 |
| 0.3381 | 150.90 | 152.52 | 154.37 | 155.73 | 156.15 | 111.92 | 112.75 | 113.69 | 114.39 | 114.60 |
| 0.3844 | 154.71 | 155.67 | 157.39 | 159.00 | 159.33 | 111.13 | 111.73 | 112.81 | 113.81 | 114.02 |
| 0.4339 | 158.09 | 159.11 | 160.52 | 161.67 | 161.95 | 110.30 | 111.09 | 112.17 | 113.04 | 113.26 |
| 0.4869 | 161.30 | 162.39 | 163.49 | 165.33 | 165.52 | 109.57 | 110.60 | 111.65 | 113.39 | 113.57 |
| 0.5438 | 164.55 | 165.07 | 166.35 | 167.29 | 167.57 | 109.18 | 109.80 | 111.32 | 112.45 | 112.78 |
| 0.6052 | 167.12 | 167.82 | 168.82 | 169.85 | 170.21 | 108.26 | 109.33 | 110.87 | 112.45 | 112.99 |
| 0.6714 | 169.93 | 170.44 | 171.51 | 172.24 | 172.81 | 108.02 | 109.08 | 111.25 | 112.75 | 113.91 |
| 0.7433 | 172.28 | 173.08 | 174.06 | 174.53 | 174.66 | 107.27 | 109.59 | 112.41 | 113.77 | 114.15 |
| 0.8214 | 174.56 | 175.36 | 175.95 | 177.35 | 177.72 | 106.62 | 110.29 | 113.02 | 119.43 | 121.14 |
| 0.9066 | 177.29 | 177.64 | 178.16 | 178.82 | 179.01 | 111.35 | 114.79 | 119.84 | 126.24 | 128.10 |
| 1.0000 | 178.82 | 179.65 | 180.11 | 180.59 | 180.69 | | | | | |

Table 8. Partial Molar Volumes $\bar{V}_1$ and $\bar{V}_2$ for the Binary System of PEG 200 and DMAPA at $T$ = (298.15, 303.15, 308.15, 313.15, and 318.15) K

| | $V_1$(PEG)/(cm$^3$·mol$^{-1}$) | | | | | $V_2$(DMAPA)/(cm$^3$·mol$^{-1}$) | | | | |
|---|---|---|---|---|---|---|---|---|---|---|
| $x_1$ | $T$/K = 298.15 | 303.15 | 308.15 | 313.15 | 318.15 | $T$/K = 298.15 | 303.15 | 308.15 | 313.15 | 318.15 |
| 0.0000 | 107.04 | 106.83 | 110.07 | 104.60 | 106.46 | 126.19 | 127.06 | 127.35 | 128.54 | 128.72 |
| 0.0262 | 116.10 | 115.48 | 118.29 | 114.01 | 115.05 | 122.82 | 123.21 | 123.74 | 124.69 | 124.43 |
| 0.0537 | 124.08 | 123.88 | 126.50 | 122.89 | 124.02 | 119.43 | 120.15 | 121.07 | 121.43 | 121.60 |
| 0.0827 | 132.04 | 132.22 | 133.97 | 131.26 | 132.09 | 117.12 | 118.13 | 118.67 | 118.86 | 119.01 |
| 0.1133 | 139.62 | 139.27 | 140.95 | 139.23 | 139.92 | 115.58 | 115.98 | 116.85 | 117.12 | 117.36 |
| 0.1455 | 146.53 | 146.40 | 147.47 | 146.70 | 147.16 | 114.57 | 115.09 | 115.68 | 116.18 | 116.37 |
| 0.1796 | 152.76 | 152.54 | 153.56 | 153.28 | 153.65 | 114.11 | 114.45 | 115.22 | 115.68 | 115.90 |
| 0.2157 | 158.30 | 158.36 | 159.07 | 159.36 | 159.62 | 114.20 | 114.73 | 115.33 | 116.00 | 116.22 |
| 0.2541 | 163.06 | 162.95 | 163.51 | 164.54 | 164.73 | 114.75 | 115.01 | 115.56 | 116.76 | 116.96 |
| 0.2948 | 167.11 | 167.18 | 167.59 | 168.65 | 168.82 | 115.79 | 116.16 | 116.59 | 117.74 | 117.94 |
| 0.3381 | 170.49 | 170.65 | 171.06 | 172.19 | 172.35 | 117.31 | 117.69 | 118.09 | 119.37 | 119.57 |
| 0.3844 | 173.12 | 173.19 | 173.65 | 174.94 | 175.11 | 119.15 | 119.37 | 119.77 | 121.35 | 121.56 |
| 0.4339 | 175.00 | 175.23 | 175.68 | 176.77 | 176.97 | 121.16 | 121.48 | 121.82 | 123.39 | 123.63 |
| 0.4869 | 176.29 | 176.69 | 177.13 | 178.47 | 178.68 | 123.35 | 123.80 | 124.09 | 126.09 | 126.36 |
| 0.5438 | 177.22 | 177.45 | 178.12 | 178.89 | 179.18 | 125.77 | 126.04 | 126.52 | 128.11 | 128.51 |
| 0.6052 | 177.53 | 177.98 | 178.61 | 179.30 | 179.66 | 127.98 | 128.50 | 128.94 | 130.52 | 131.05 |
| 0.6714 | 177.91 | 178.35 | 179.10 | 179.51 | 180.02 | 130.56 | 131.16 | 131.72 | 133.00 | 133.73 |
| 0.7433 | 178.09 | 178.83 | 179.55 | 179.76 | 179.92 | 133.28 | 134.35 | 134.84 | 135.82 | 136.21 |
| 0.8214 | 178.41 | 179.22 | 179.65 | 180.68 | 180.97 | 136.90 | 138.35 | 138.29 | 140.06 | 140.40 |
| 0.9066 | 179.30 | 179.74 | 180.11 | 180.68 | 180.78 | 142.95 | 144.51 | 143.68 | 145.31 | 144.91 |
| 1.0000 | 178.82 | 179.65 | 180.11 | 180.59 | 180.69 | 151.91 | 154.62 | 152.19 | 154.99 | 153.27 |

of $T$ = (298.15, 303.15, 308.15, 313.15, and 318.15) K at atmospheric pressure were reported. The density and viscosity data have been used to compute the parameter of excess properties and viscous flow thermodynamics. The $V_m^E$ values were negative, $\Delta\eta$ is not always negative, it also shows a positive maximum and a negative minimum at around $x_1 \approx 0.6067$ and $x_1 \approx 0.1158$; meanwhile, the $\Delta H^*$, $\Delta S^*$, and $\Delta G^*$ values were calculated. Based on the results of $V_m^E$, it was found that a stronger intermolecular bonding is formed. A mixture of PEG 200 and DMAPA in a ratio of 1:2 was used for investigating $CO_2$ absorption at a pressure of 1 bar, and a $CO_2$ absorption of about 0.19 g per gram of the absorbent at room temperature was achieved. In addition, the UV−vis, FTIR, and $^1$H NMR results indicate that there are hydrogen bonding and interactions of hydroxyl hydrogen atoms in PEG 200 with nitrogen atoms in DMAPA leading to the formation of $(CH_3)_2N\cdots HOCH_2CH-O-$ and $H_2N\cdots HOCH_2CH-O-$.



https://doi.org/10.1021/acsomega.1c00667
ACS Omega 2021, 6, 9898−9909

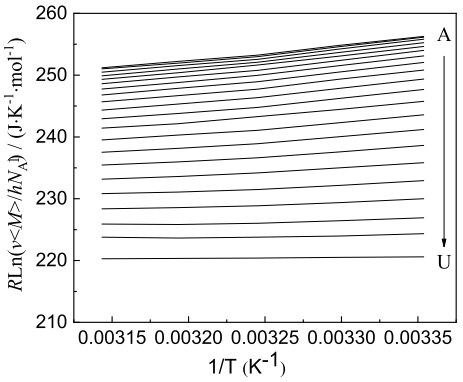


**Figure 8.** Plots of $R\ \ln(\nu M/\mathrm{hNA})$ against $1/T$ for PEG 200 (**1**) + DMAPA (**2**) at different temperatures, and the molar fractions corresponding to lines are as follows: ($A$: $x_1$ = 0.0000 ∼ $U$: $x_1$ = 1.0000).

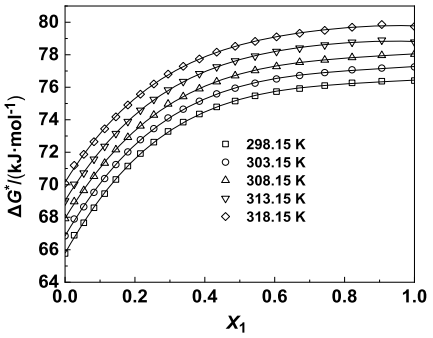


**Figure 9.** Gibbs free energies of activation ($\Delta G^*$) with the mole fraction for the viscous flow of PEG 200 (**1**) + DMAPA (**2**) at $T$ = (298.15, 303.15, 308.15, 313.15, and 318.15) K and atmospheric pressure. The symbols represent experimental values, and the solid curves represent the values calculated from eq 7.

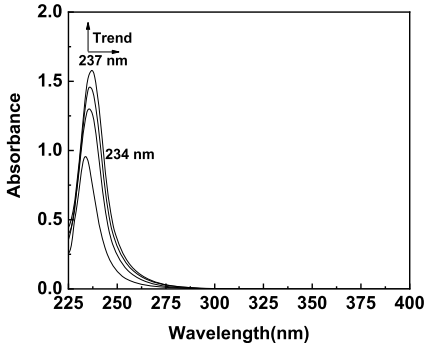


**Figure 10.** UV−vis spectral changes with increasing DMAPA concentration in the binary system of PEG 200 (**1**) + DMAPA (**2**).

These results are helpful to understand and optimize the $CO_2$ absorption capacity of the binary solution.

## 4. EXPERIMENTAL SECTION

**4.1. Materials.** Analytical grade DMAPA (≥99.0%) and PEG 200 (≥99.0%) were purchased from Shanghai Titan Technology Co., Ltd., China. They were dried over 4 Å molecular sieves and degassed by ultrasonication just before the experiment. The water contents of PEG 200 and DMAPA were determined by the Carl Fischer method to be 0.21 and 0.07 wt %, respectively. Moreover, double-distilled water and HPLC grade ethanol were used to calibrate the pycnometer and the Ubbelohde viscometer, respectively. All specifications of chemical samples are shown in Table S1.

**4.2. Instrumentation.** All measurements of mass were performed on an electronic balance with an accuracy of ±0.1 mg (Sartorius BS224S). The uncertainty of mole fraction was estimated to be ±0.0001. The UV−vis spectra were recorded on a Shimadzu UV-3600 plus spectrometer. FTIR spectra

**Table 9. Gibbs Free Energy Changes ($\Delta G^*$/kJ·mol$^{-1}$), Enthalpy of Activation ($\Delta H^*$), and Entropy of Activation ($\Delta S^*$) for the Viscous Flow of the Binary System PEG 200 (1) + DMAPA (2) at Different Concentrations**

| | | | $\Delta G^*$/(kJ·mol$^{-1}$) | | | | |
|---|---|---|---|---|---|---|---|
| $x_1$ | $\Delta H^*$/(kJ·mol$^{-1}$) | $\Delta S^*$/(J·mol$^{-1}$·K$^{-1}$) | $T/K$ = 298.15 | 303.15 | 308.15 | 313.15 | 318.15 |
| 0.0000 | 1.51 ± 0.087 | −215.52 ± 0.28 | 65.77 | 66.85 | 67.92 | 69.00 | 70.08 |
| 0.0262 | 2.83 ± 0.99 | −214.73 ± 3.23 | 66.89 | 67.89 | 68.96 | 70.03 | 71.19 |
| 0.0537 | 5.07 ± 1.18 | −209.77 ± 3.84 | 67.66 | 68.64 | 69.65 | 70.72 | 71.87 |
| 0.0827 | 7.80 ± 0.92 | −203.70 ± 3.00 | 68.58 | 69.53 | 70.52 | 71.57 | 72.65 |
| 0.1133 | 10.07 ± 1.08 | −199.00 ± 3.50 | 69.45 | 70.38 | 71.33 | 72.36 | 73.44 |
| 0.1455 | 12.86 ± 0.86 | −192.61 ± 2.79 | 70.32 | 71.24 | 72.16 | 73.15 | 74.18 |
| 0.1796 | 15.17 ± 1.13 | −187.60 ± 3.66 | 71.15 | 72.02 | 72.92 | 73.89 | 74.91 |
| 0.2157 | 17.64 ± 1.22 | −181.89 ± 3.95 | 71.92 | 72.77 | 73.62 | 74.58 | 75.57 |
| 0.2541 | 19.26 ± 1.20 | −178.82 ± 3.88 | 72.62 | 73.45 | 74.29 | 75.25 | 76.20 |
| 0.2948 | 20.91 ± 0.97 | −175.52 ± 3.15 | 73.28 | 74.11 | 74.97 | 75.83 | 76.81 |
| 0.3381 | 22.68 ± 1.35 | −171.45 ± 4.37 | 73.85 | 74.65 | 75.43 | 76.35 | 77.29 |
| 0.3844 | 23.95 ± 1.21 | −168.90 ± 3.92 | 74.35 | 75.14 | 75.91 | 76.83 | 77.74 |
| 0.4339 | 24.64 ± 1.26 | −168.05 ± 4.10 | 74.79 | 75.59 | 76.34 | 77.25 | 78.16 |
| 0.4869 | 25.06 ± 1.16 | −167.88 ± 3.77 | 75.15 | 75.94 | 76.71 | 77.62 | 78.52 |
| 0.5438 | 25.60 ± 1.10 | −167.11 ± 3.58 | 75.47 | 76.25 | 77.03 | 77.92 | 78.82 |
| 0.6052 | 25.55 ± 1.27 | −168.13 ± 4.13 | 75.73 | 76.51 | 77.28 | 78.20 | 79.10 |
| 0.6714 | 25.37 ± 0.82 | −169.45 ± 2.65 | 75.92 | 76.72 | 77.54 | 78.41 | 79.32 |
| 0.7433 | 25.49 ± 1.10 | −169.62 ± 3.57 | 76.10 | 76.90 | 77.68 | 78.60 | 79.50 |
| 0.8214 | 25.40 ± 1.43 | −170.45 ± 4.63 | 76.27 | 77.07 | 77.83 | 78.77 | 79.69 |
| 0.9066 | 24.56 ± 1.45 | −173.60 ± 4.70 | 76.37 | 77.18 | 77.96 | 78.90 | 79.86 |
| 1.0000 | 27.63 ± 1.18 | −163.61 ± 3.85 | 76.41 | 77.25 | 78.04 | 78.78 | 79.74 |



https://doi.org/10.1021/acsomega.1c00667
ACS Omega 2021, 6, 9898−9909

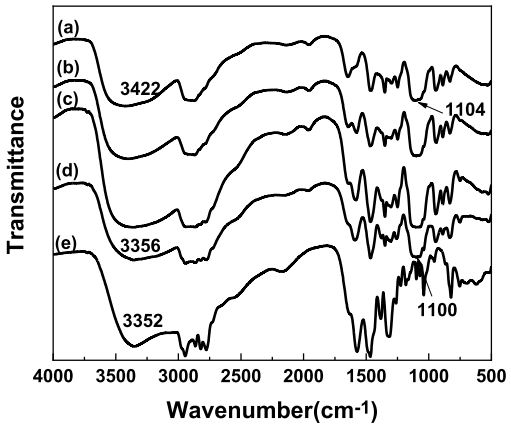


**Figure 11.** FTIR spectra of (a) PEG 200, (b) PEG 200 + DMAPA (2:1 mole ratio), (c) PEG 200 + DMAPA (1:1 mole ratio), (d) PEG 200 + DMAPA (1:2 mole ratio), and (e) DMAPA.

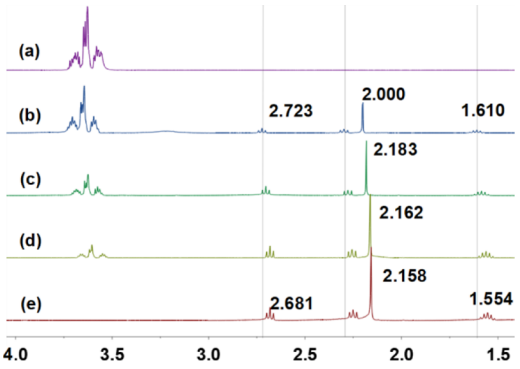


**Figure 12.** $^1$H NMR spectra of (a) PEG 200, (b) PEG 200 + DMAPA (2:1 mole ratio), (c) PEG 200 + DMAPA (1:1 mole ratio); (d) PEG 200 + DMAPA (1:2 mole ratio), and (e) DMAPA.

were recorded on a Nicolet 50 FTIR spectrometer. $^1$H NMR spectra were recorded on a JNM-ECZ-400 spectrometer. All spectral experiments of PEG 200 (**1**) + DMAPA (**2**) were performed at room temperature and atmospheric pressure.

**4.3. Measurements.** The density of the sample was measured by the pycnometer method. Briefly, the pycnometer containing the binary solvent solution was placed in a constant temperature water bath at a desired temperature for 30 min, and then weighed at least three times to obtain the average value. The uncertainty of density measurement was estimated to be ±0.02%. The viscosity of the sample was measured using an Ubbelohde viscometer. First, the Ubbelohde viscometer was calibrated with double-distilled water and HPLC grade ethanol, and the viscometer constant was calculated. A stopwatch was used to measure the time when the liquid flows through the capillary of the viscometer and this was repeated at least six times for each sample to obtain the average value. The uncertainty of the viscosity value was ±3%. In order to determine the reliability of the experiment, the experimentally measured values of density and absolute viscosity of DMAPA and PEG 200 are compared with those reported in the literature,[30−35] as shown in Table S2. The agreement between the experimental and literature values was found to be satisfactory.

**4.4. Absorption of $CO_2$.** The bubble weight method was used in the experiment of $CO_2$ absorption. In short, $CO_2$ absorption was carried out at room temperature at a pressure of 1 bar. As shown in Figure S1, a known amount of absorbent was placed in a glass tube (inner diameter: 10 mm; length: 200 mm). The gas containing $CO_2$ is bubbled into the absorption solution through a long stainless-steel needle. During gas absorption, the gas solubility was determined by weighing the tube on an electronic analytical balance (Sartorius BS224S). To ensure balance is achieved, the weighing procedure was repeated until the mass remains constant between successive measurements. For diluted $CO_2$ absorption, in a typical procedure, about 2.0 g of absorbent was added to a U-shaped absorption tube with an inner diameter of 8 mm, and then the absorption tube was placed in a 25 °C water bath. The $CO_2$ gas (10 wt %) was controlled by a mass flow meter to control the flow rate to 30 mL·min$^{-1}$. $CO_2$ was absorbed by the absorbent when it passed through the U-shaped tube. Then, the concentration of the $CO_2$ tail gas was detected using the flue gas analyzer (LY800-$CO_2$, Shenzhen Liye Industrial Co., LTD. China) and the change in $CO_2$ concentration was recorded online using a computer.

## ■ ASSOCIATED CONTENT

### Supporting Information

The Supporting Information is available free of charge at https://pubs.acs.org/doi/10.1021/acsomega.1c00667.

Specification of chemical samples; comparison of experimental density and viscosity values of pure PEG and DMAPA with literature values at different temper-

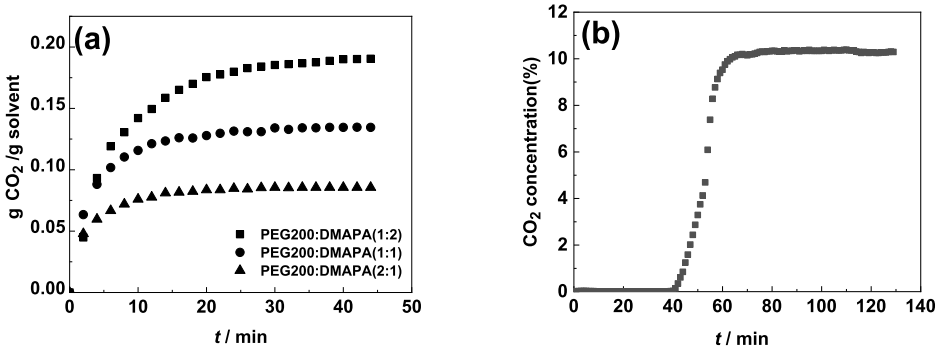


**Figure 13.** (a) Comparison of $CO_2$ absorption processes by the amide-based binary system of PEG 200 (**1**) + DMAPA (**2**) as a function of time at 25 °C and 1.0 bar; (b) $CO_2$ (10 wt %) + $N_2$ removal efficiency as a function of time at 25 °C and 1.0 bar in PEG 200 plus DMAPA (1:2 mole ratio).



https://doi.org/10.1021/acsomega.1c00667
ACS Omega 2021, 6, 9898−9909

atures; and experimental diagram for $CO_2$ absorption (PDF)

## AUTHOR INFORMATION


### Corresponding Authors

**Tianxiang Zhao** − *Key Laboratory of Green Chemical and Clean Energy Technology, School of Chemistry and Chemical Engineering, Guizhou University, Guiyang 550025, P. R. China*; orcid.org/0000-0001-8197-2423; Email: txzhao3@gzu.edu.cn

**Fei Liu** − *Key Laboratory of Green Chemical and Clean Energy Technology, School of Chemistry and Chemical Engineering, Guizhou University, Guiyang 550025, P. R. China*; Email: ce.feiliu@gzu.edu.cn

### Authors

**Xiaoqing Yang** − *Key Laboratory of Green Chemical and Clean Energy Technology, School of Chemistry and Chemical Engineering, Guizhou University, Guiyang 550025, P. R. China*

**Zimin Liu** − *Key Laboratory of Green Chemical and Clean Energy Technology, School of Chemistry and Chemical Engineering, Guizhou University, Guiyang 550025, P. R. China*

**Jiarui Gu** − *Key Laboratory of Green Chemical and Clean Energy Technology, School of Chemistry and Chemical Engineering, Guizhou University, Guiyang 550025, P. R. China*

**Jianxin Cao** − *Key Laboratory of Green Chemical and Clean Energy Technology, School of Chemistry and Chemical Engineering, Guizhou University, Guiyang 550025, P. R. China*

Complete contact information is available at: https://pubs.acs.org/10.1021/acsomega.1c00667

### Author Contributions

†X.Y. and Z.L. authors contributed equally.


### Notes

The authors declare no competing financial interest.

## ACKNOWLEDGMENTS

This work was supported by Natural Science Special Foundation of Guizhou University (no. X2019065 Special Post A), Guizhou University Cultivation Project (no.201955), Characteristic Field Project of Education Department in Guizhou Province (no. 2021055), Scientific and Technological Innovation Talents Team Project of Guizhou Province (no. 20185607), One Hundred Person Project of Guizhou Province (no. 20165655), Innovation Group Project of Education Department in Guizhou Province (no. 2021010), and the Guizhou Province Graduate Research Fund (no.2020044).

## REFERENCES


(1) Heldebrant, D. J.; Koech, P. K.; Glezakou, V.-A.; Rousseau, R.; Malhotra, D.; Cantu, D. C. Water-lean solvents for post-combustion $CO_2$ capture: Fundamentals, uncertainties, opportunities, and outlook. *Chem. Rev.* **2017**, *117*, 9594−9624.

(2) Chen, T.; Ma, J.; Chen, S.; Wei, Y.; Deng, C.; Chen, J.; Hu, J.; Ding, W. Construction of heterostructured CoP/CN/Ni: Electron redistribution towards effective hydrogen generation and oxygen reduction. *Chem. Eng. J.* **2021**, *415*, 129031.

(3) Karlsson, H. K.; Makhool, H.; Karlsson, M.; Svensson, H. Chemical absorption of carbon dioxide in non-aqueous systems using the amine 2-amino-2-methyl-1-propanol in dimethyl sulfoxide and N-methyl-2-pyrrolidone. *Sep. Purif. Technol.* **2021**, *256*, 117789.

(4) Olah, G. A.; Mathew, T.; Prakash, G. K. S. Chemical formation of methanol and hydrocarbon ("organic") derivatives from $CO_2$ and $H_2$ carbon sources for subsequent biological cell evolution and Life's origin. *J. Am. Chem. Soc.* **2017**, *139*, 566−570.

(5) Peng, H.-L.; Zhang, J.-B.; Zhang, J.-Y.; Zhong, F.-Y.; Wu, P.-K.; Huang, K.; Fan, J.-P.; Liu, F. Chitosan-derived mesoporous carbon with ultrahigh pore volume for amine impregnation and highly efficient $CO_2$ capture. *Chem. Eng. J.* **2019**, *359*, 1159−1165.

(6) Zhao, J.; Shan, W.; Zhang, P.; Dai, S. Solvent-free and mechanochemical synthesis of N-doped mesoporous carbon from tannin and related gas sorption property. *Chem. Eng. J.* **2020**, *381*, 122579.

(7) Zhang, X.; Xiong, W.; Tu, Z.; Peng, L.; Wu, Y.; Hu, X. Supported Ionic Liquid Membranes with Dual-Site Interaction Mechanism for Efficient Separation of $CO_2$. *ACS Sustainable Chem. Eng.* **2019**, *7*, 10792−10799.

(8) Tu, Z.; Liu, P.; Zhang, X.; Shi, M.; Zhang, Z.; Luo, S.; Zhang, L.; Wu, Y.; Hu, X. Highly-selective separation of $CO_2$ from $N_2$ or $CH_4$ in task-specific ionic liquid membranes: Facilitated transport and salting-out effect. *Sep. Purif. Technol.* **2021**, *254*, 117621.

(9) Hedayati, A.; Feyzi, F. $CO_2$-binding organic liquids comprised of 1,1,3,3-tetramethylguanidine and alkanol for postcombustion $CO_2$ capture: water inhibitory effect of amine promoters. *ACS Sustainable Chem. Eng.* **2020**, *8*, 7909−7920.

(10) Hedayati, A.; Feyzi, F. Towards water-insensitive $CO_2$-binding organic liquids for $CO_2$ absorption: Effect of amines as promoter. *J. Mol. Liq.* **2020**, *306*, 112938.

(11) Zhang, J.-B.; Peng, H.; Liu, Y.; Tao, D.-J.; Wu, P.; Fan, J.-P.; Huang, K. Highly efficient $CO_2$ capture by polyethylenimine plus 1-ethyl-3-methylimidazolium acetate mixed absorbents. *ACS Sustainable Chem. Eng.* **2019**, *7*, 9369−9377.

(12) Karlsson, H. K.; Sanku, M. G.; Svensson, H. Absorption of carbon dioxide in mixtures of N-methyl-2-pyrrolidone and 2-amino-2-methyl-1-propanol. *Int. J. Greenhouse Gas Control* **2020**, *95*, 102952.

(13) Kortunov, P. V.; Siskin, M.; Paccagnini, M.; Thomann, H. $CO_2$ reaction mechanisms with hindered alkanolamines: control and promotion of reaction pathways. *Energy Fuels* **2016**, *30*, 1223−2123.

(14) Heldebrant, D. J.; Yonker, C. R.; Jessop, P. G.; Phan, L. Organic liquid $CO_2$ capture agents with high gravimetric $CO_2$ capacity. *Energy Environ. Sci.* **2008**, *1*, 487−493.

(15) Zhao, T.; Guo, B.; Han, L.; Zhu, N.; Gao, F.; Li, Q.; Li, L.; Zhang, J. Agile $CO_2$ fixation into novel $CO_2$-storage materials from 1,2-ethanediamine and ethylene glycol derivatives. *ChemPhysChem* **2015**, *16*, 2106−2109.

(16) Yang, D.; Lv, M.; Chen, J. Efficient non-aqueous solvent formed by 2-piperidineethanol and ethylene glycol for $CO_2$ absorption. *Chem. Commun.* **2019**, *55*, 12483−12486.

(17) Chen, T.; Xu, Y.; Guo, S.; Wei, D.; Peng, L.; Guo, X.; Xue, N.; Zhu, Y.; Chen, Z.; Zhao, B.; Ding, W. Ternary heterostructural Pt/CN/Ni as a supercatalyst for oxygen reduction. *iScience* **2019**, *11*, 388−397.

(18) Li, J.; Chen, L.; Ye, Y.; Qi, Z. Solubility of $CO_2$ in the mixed solvent system of alkanolamines and poly(ethylene glycol) 200. *J. Chem. Eng. Data* **2014**, *59*, 1781−1787.

(19) Chen, Y.; Hu, H. Carbon dioxide capture by diethylenetriamine hydrobromide in nonaqueous systems and phase-change formation. *Energy Fuels* **2017**, *31*, 5363−5375.

(20) Zheng, W.-T.; Huang, K.; Wu, Y.-T.; Hu, X.-B. Protic ionic liquids as excellent shuttle of MDEA for fast capture of $CO_2$. *AIChE J.* **2018**, *64*, 209−219.

(21) Heldebrant, D. J.; Koech, P. K.; Rainbolt, J. E.; Zheng, F.; Smurthwaite, T.; Freeman, C. J.; Oss, M.; Leito, I. Performance of single-component $CO_2$-binding organic liquids ($CO_2$BOLs) for post combustion $CO_2$ capture. *Chem. Eng. J.* **2011**, *171*, 794−800.

(22) Zhao, T.; Zhang, J.; Guo, B.; Zhang, F.; Sha, F.; Xie, X.; Wei, X. Density, viscosity and spectroscopic studies of binary system ethylene glycol + dimethyl sulfoxide at $T$ = (298.15 to 323.15) K. *J. Mol. Liq.* **2015**, *207*, 315−322.
(23) del Carmen Grande, M.; Juliá, J. A.; García, M.; Marschoff, C. M. On the density and viscosity of (water + dimethylsulfoxide) binary mixtures. *J. Chem. Thermodyn.* **2007**, *39*, 1049−1056.
(24) Živković, N. V.; Šerbanović, S. S.; Kijevčanin, M. L.; Živković, E. M. Volumetric and viscometric behavior of binary systems 2-butanol + PEG200, + PEG 400, + tetraethylene glycol dimethyl ether, and + N-methyl-2-pyrrolidone. *J. Chem. Eng. Data* **2013**, *58*, 3332−3341.
(25) Ali, A.; Ansari, S.; Nain, A. K. Densities, refractive indices and excess properties of binary mixtures of dimethylsulfoxide with some poly-(ethylene glycol)s at different temperatures. *J. Mol. Liq.* **2013**, *178*, 178−184.
(26) Billah, M. M.; Rocky, M. M. H.; Hossen, I.; Hossain, I.; Hossain, M. N.; Akhtar, S. Densities, viscosities,and refractive indices for the binary mixtures of tri-n-butyl phosphate (TBP) with toluene and ethylbenzene between (303.15 and 323.15) K. *J. Mol. Liq.* **2018**, *265*, 611−620.
(27) Li, B.; Zhao, L.; Yue, X.; Pang, Y.; Zhang, S.; Wu, Z.; Zhang, J. Density, viscosity and intermolecular interaction of polyethylene glycol 300 + N, N-dimethylformamide binary mixture. *Phys. Chem. Liq.* **2021**, *59*, 90−103.
(28) Zhang, Q.; Li, Q.; Liu, D.; Zhang, X.; Lang, X. Density, dynamic viscosity, electrical conductivity, electrochemical potential window, and excess properties of ionic liquid N-butyl-pyridinium dicyanamide and binary system with propylene carbonate. *J. Mol. Liq.* **2018**, *249*, 1097−1106.
(29) Dubey, G. P.; Sharma, M.; Dubey, N. Study of densities, viscosities, and speeds of sound of binary liquid mixtures of butan-1-ol with n-alkanes ($C_6$, $C_8$, and $C_{10}$) at $T$ = (298.15, 303.15, and 308.15) K. *J. Chem. Thermodyn.* **2008**, *40*, 309−320.
(30) Zhao, T.; Feng, X.; Zheng, W.; Hu, X.; Zhang, J.; Wu, Y. Solubility of dilute $SO_2$ in binary system of polyethylene glycol 200 and dimethyl sulfoxide as a function of liquid composition and system's spectroscopic studies. *J. Mol. Liq.* **2017**, *225*, 151−159.
(31) Blanco, A.; García-Abuín, A.; Gómez-Díaz, D.; Navaza, J. M. Density, speed of sound, viscosity and surface tension of 3-dimethylamino-1-propylamine + water, 3-amino-1-propanol +3-dimethylamino-1-propanol, and (3-amino-1-propanol + 3-dimethylamino-1-propanol) + water from $T$ = (293.15 to 323.15) K. *J. Chem. Eng. Data* **2017**, *62*, 2272−2279.
(32) Du, W.; Wang, X. Density and viscosity for binary mixtures of methyl decanoate with 1-propanol, 1-butanol, and 1-pentanol. *J. Mol. Liq.* **2019**, *294*, 111647.
(33) Li, L.; Zhang, J.; Li, Q.; Guo, B.; Zhao, T.; Sha, F. Density, viscosity, surface tension, and spectroscopic properties for binary system of 1,2-ethanediamine + diethylene glycol. *Thermochim. Acta* **2014**, *590*, 91−99.
(34) Jia, X.; Zhang, S.; Li, B.; Yang, J.; Zhang, J.; Fu, J. Density, viscosity, surface tension and intermolecular interaction of triethylene glycol and 1,2-diaminopropane binary solution & its potential downstream usage for bioplastic production. *J. Mol. Liq.* **2020**, *306*, 112804.
(35) Pal, A.; Kumar, A. Excess molar volumes and viscosities of binary mixtures of 2-(2-butoxyethoxy) ethanol with chloroalkanes at 298.15 K. *Fluid Phase Equilib.* **1998**, *143*, 241−251.


https://doi.org/10.1021/acsomega.1c00667
*ACS Omega* 2021, 6, 9898−9909